Search for New Physics in All-hadronic Events with AlphaT in 8 TeV data at CERN

Yossof Eshaq

Submitted in Partial Fulfillment of the

Requirements for the Degree Doctor of Philosophy

Supervised by Professor Aran Garcia-Bellido

Department of Physics

Astronomy

Arts, Sciences and Engineering

University of Rocheser

October 2, 2014

Abstract

An inclusive search for supersymmetric processes that produce final states with jets and missing transverse energy is performed in pp collisions at a centre-of-mass energy of $\sqrt{s} = 8\,\mathrm{TeV}$. The data sample corresponds to an integrated luminosity of $18.5\,\mathrm{fb}^{-1}$ collected by the CMS experiment at the LHC. In this search, a dimensionless kinematic variable, α_{T}, is used to discriminate between events with genuine and misreconstructed missing transverse energy. The search is based on an examination of the number of reconstructed jets per event, the scalar sum of transverse energies of these jets, and the number of these jets identified as originating from bottom quarks. The results are interpreted with various simplified models, with a special emphasis on models with a compressed mass spectrum.

0.1 Theoritical motivation

SM,Higgs,SUSY

Particle physics concerns itself with the study of particles and fields. Our current knowledge of their charactericts and interactions are formalized the quantum field theory called the Standard Model. I through three symmetries: The color charge symmetry of Quantum Chromo Dynamics (QCD) represented in SU(3), the flavor symemmetry of Quantum Flavor Dynamics (QFD) represented in SU(2) and the electric charge symmetry of Quantum Electro Dynamics represented in U(1). Together, SU(3)XSU(2)XU(1) represent the field theory.

0.2 LHC and CMS

LHC, CMS

0.3 Definition of $\alpha_{\mathbf{T}}$

0.4 Data sets and Monte Carlo samples

0.4.1 Data sets

The data analysed consist of the full run of 2012.

The following datasets are used to populate the hadronic signal and control samples. They correspond to the full data run of 2012 and an integrated luminosity of $19.45 \pm 0.8\,\mathrm{fb}^{-1}$. The official JSON from the 22$^{\mathrm{nd}}$ Jan 2013 is used to filter only certified luminosity sections with the run range 190456–208686.

Table 1: Datasets.

Dataset	Luminosity (fb^{-1})
Hadronic	19.45
Muon	19.72
Photon	19.63

0.4.2 MC samples for signal and SM backgrounds

The SM background Monte Carlo samples for physics at 8 TeV are taken from the `Summer12` simulation production run with `CMSSW_5_3_X` with the `PU_S10` scenario. The effective luminosity of each MC sample is normalised to the integrated luminosity of the corresponding dataset, as listed in Table 2. The signal MADGRAPH Monte Carlo samples, listed in Table **??**, are taken from a `FastSim` simulation production based on `CMSSW_5_2_X`. All MC samples are reweighted on an event-by-event basis such that the distribution of pile-up (PU) interactions matches that observed in data. This is done using the recommended recipe and the PU JSON of 13$^{\mathrm{th}}$ December 2012.

Table 2: MC samples for Standard Model processes.

Sample	HT (GeV)	Cross section (pb)	Corrected Cross section (pb)
W $\to l\nu$	Inclusive	37509.0	34133.2
W $\to l\nu$	150 - 200	253.8	234.53
W $\to l\nu$	200 - 250	116.5	103.94
W $\to l\nu$	250 - 300	57.6	51.34
W $\to l\nu$	300 - 400	48.4	42.41
W $\to l\nu$	400 - ∞	30.8	26.36
Z $\to \nu\bar{\nu}$	50 - 100	452.8	405.21
Z $\to \nu\bar{\nu}$	100 - 200	190.4	173.76
Z $\to \nu\bar{\nu}$	200 - 400	45.1	42.41
Z $\to \nu\bar{\nu}$	400 - ∞	6.26	5.81
$t\bar{t}$	Inclusive	234.0	271.44
Z/$\gamma^* \to l^+l^-(m_{ll} > 50)$	Inclusive	3503.7	3258.45
Z/$\gamma^* \to l^+l^-(10 < m_{ll} < 50)$	Inclusive	13124.1	12205.4
Z/$\gamma^* \to l^+l^-$	200 - 400	24.3	22.24
Z/$\gamma^* \to l^+l^-$	400 - ∞	3.36	3.11
γ + jets	200 - 400	1140.8	1060.9
γ + jets	400 - ∞	124.7	115.97
WW	Inclusive	57.1	57.1
WZ	Inclusive	12.6	12.6
ZZ	Inclusive	8.26	8.26
t (t-channel)	Inclusive	56.4	56.4
$\bar{\text{t}}$ (t-channel)	Inclusive	30.7	30.7
t (s-channel)	Inclusive	3.79	3.79
$\bar{\text{t}}$ (s-channel)	Inclusive	1.76	1.76
t (tW-channel)	Inclusive	11.1	11.1
$\bar{\text{t}}$ (tW-channel)	Inclusive	11.1	11.1

0.4.3 Corrections to cross sections for SM samples

A simulated event is weighted by the total numer of events in the MC sample, the thoeritical cross section, and total luminosiy of the data being studied. The MC Pog provides next-to-next-to leading order (NNLO) thoeritical cross section for un-filtered (inclusive) SM samples [**?**]. In an attempt to provide higher statistics in tails of distrubtion analyses often cut on (ie $H_{\mathrm{T}}^{\mathrm{parton}}$, N^{parton}, $\hat{p}_T$), MC samples are provided binned in these variables. Only the leading-order (LO) cross sections are provided [**?**] but in general, the k-factors required to go from LO to NNLO cross sections are determined using corresponding inclusive samples and applied to each binned sample.

Studies conducted by other analyses [**?**] revealed that some LO cross sections calculated for MC samples binned according to $H_{\mathrm{T}}^{\mathrm{parton}}$ are inaccurate to a level as large as 10%, leading to non-physical discontinuities in the $H_{\mathrm{T}}^{\mathrm{parton}}$ distribution constructed from the binned samples of a given process. Futhermore, due to an error in production, the $\mathrm{W} \rightarrow l\nu \quad H_{\mathrm{T}}$ binned samples exhibit H_{T}-depended biases. The following paragraphs describes a procedure to measure corrections to the discontinuites and biases of the $\mathrm{W} \rightarrow l\nu \quad H_{\mathrm{T}}{}^{\mathrm{parton}}$ binned samples as a function of H_{T}. Other analyses created similar procedures to correct the $\mathrm{Z} \rightarrow \mu\mu \quad H_{\mathrm{T}}{}^{\mathrm{parton}}$ binned samples, this analysis uses those measured corrections as k-factors.

As a first step, we wish to reweigh the cross sections of the $H_{\mathrm{T}}{}^{\mathrm{parton}}$ binned samples such that their $H_{\mathrm{T}}{}^{\mathrm{parton}}$ distributions match that of the inclusive sample's. Due to the inclusive sample's limited statitistics in the tails of H_{T} distribution, we instead use the N^{parton} binned's $H_{\mathrm{T}}{}^{\mathrm{parton}}$ distribution which is verified to agree well with the inclusive sample figure 1 (a). Additionally, to smooth statistical flucutations, both distributions are fitted using a double exponetional of the form $exp(a + b * x + c * x^{1.05})$ for $H_{\mathrm{T}} > 500\,\mathrm{GeV}$ figure 1 (b). The ratio of the distributions figure 1(c) is applied as $H_{\mathrm{T}}{}^{\mathrm{parton}}$ dependent event weight.

In the high-H_{T} and high-$\not{E}_{\mathrm{T}}$ corner of kinematic phase space of this analysis (and other SUSY analyses) the overall normalization of MC samples do not agree well with data. Therefore a data sideband in H_{T} is used to determine sample-specific corrections that are appropriate for the H_{T}-$\not{E}_{\mathrm{T}}$ phase space covered by this analysis. This correction is determined for the $\mathrm{W} \rightarrow l\nu$ and $t\bar{t}$ samples by impososing requirements on the number of muons, jets, and b-tagged jets, to obtain samples rich in W + jets, and $t\bar{t}$ events. A sideband in H_{T} is used to determine both the yields in data and MC expectations. The sideband is defined by the region $200 < H_{\mathrm{T}} < 225\,\mathrm{GeV}$ and uses the jet p_{T} thresholds $(73, 73, 37\,\mathrm{GeV})$ to maintain comparable jet multiplicities, kinematics. and background admixtures as observed for the higher HT bins. Trigger efficiency and b-tag scale factor corrections are determined and applied to the MC samples. The purity of the samples are $> 80\%$ and any contamination is taken into account. The correction is determined by taking the ratio of the data yield over the MC expectation in the sideband. Table 3 summarises the selection and corrections for the different samples.

Table 3: Correctins determined from a data sideband for the W + jets and $t\bar{t}$ samples. “Corrected yield” reflects the observed data yield minus the contamination as given by MC.

Process	Selection	Purity	Corrected yield	MC expectation	Correction Factor
W + jets	μ + jets, $2 \leq n_{\text{jet}} \leq 3$, $n_{\text{b}} = 0$	0.90	15682	18013.1 ± 85.9	0.87 ± 0.01
$t\bar{t}$	μ + jets, $n_{\text{jet}} \geq 2$, $n_{\text{b}} \geq 2$	0.83	752	736.7 ± 11.5	1.02 ± 0.05

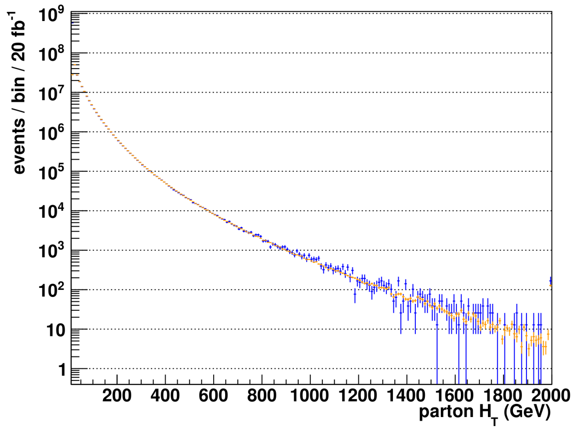

(a) Parton H_{T} distrbution for the $\mathrm{W} \rightarrow l\nu$ inclusive sample (blue) and $\mathrm{W} \rightarrow l\nu\ N^{\mathrm{parton}}$ binned sample (orange.)

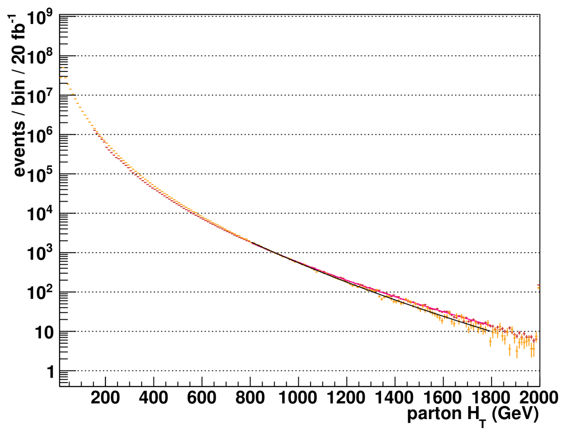

(b) Fitted Parton H_{T} distrbution for the $\mathrm{W} \rightarrow l\nu\ H_{\mathrm{T}}{}^{\mathrm{parton}}$ sample (purple) and $\mathrm{W} \rightarrow l\nu\ N^{\mathrm{parton}}$ binned sample (orange.)

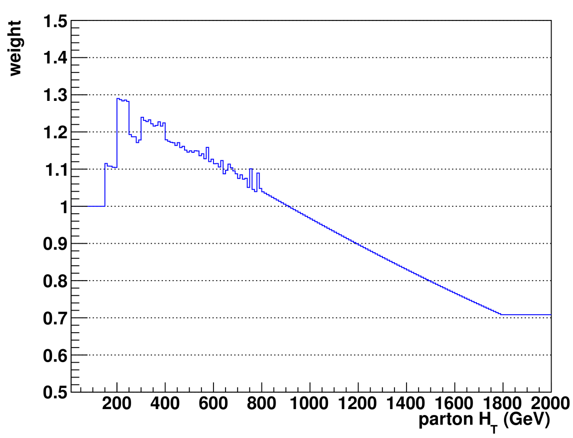

(c) Event weight determined from ration of figure 1 (b)

Figure 1: Generator-level $H_{\mathrm{T}}{}^{\mathrm{parton}}$ distributions and measured weights

0.5 Hadronic Event Selection

As discused in [REF], all-hadronic SUSY signatures consist of events with no isolated and detectable objects apart from energetic jets. To search for an excess in such events, it is convenient to use a jet-based variable, H_{T}, to quantify the energy in an event. H_{T} is defined as the scalar sum of the transverse energy of the jets in the event. The challanges due to large backgrounds in a search for an excess in all-hadronic events becomes evident when compairing observed data events overlaid with simulated events from SM processes as a function of H_{T} Figure [REF].

The dominant background are azimuthally-balanced multi-jet events, stemming from QCD processes. This search reduces this background to negligible levels in the selected region by employing the α_{T} variable further discussd in section [REF]. Furthermore, by construction, α_{T} also reduces backgrounds from severely mis-measured jets.

In absence of the multi-jet background, the remaining significant backgrounds are ...

0.5.1 Data

The data analyzed was recorded by CMS in 2012 between April 5th and Dec. 5th and totals 19.47$\pm$ 2.6%. The collected data is certified on a run-by-run basis, where initial automatic certification requires the LHC beams to be declared stable and all CMS subdetectors ON. Further monitoring of the data was done realtime by experts of each subdetector trough analysis of histograms updated and filled each lumi section. Final cerfitication was done offline, and lumi sections passing all criteria were listed in a Golden JSON file to be used by all analyses.

0.5.2 Event quality

Each event is subjected to a series of commonly used filters in CMS to ensure good quality data. Minimal requirements are that at least one primary vertex is identified and 25% of the reconstructed tracks to be of good quality. Addionally, various filters prescribed by the MET group[REF] are applied. Events containing muons with inconsistent energy are flagged by the muon pog [REF] and filtered out of the analysis.

0.5.3 Triggers

Hadronic signal region and control samples

Only events passing one or more HLT triggers based on online quantanties are recorded to be analyzed. For any analysis, in general, it is not expected that all recorded events reconstructed offline, pass the online trigger as detector conditions, energy corrections, and object-based quantaties differ offline. In this analysis, cross-triggers at the HLT based on quantities H_{T} and α_{T} (labelled as `HTxxx_AlphaT0pyy`) are used with various thresholds to record candidate events for the hadronic (signal) region. In order to keep the cross-trigger's computational time low, the online quantaties are constructed using simple calorimeter based jets (calo jets), and the use of partcle-flow jets in this analysis is expected to introduce inefficiencies.

Each H_{T} bin is seeded by a single trigger chosen based on the efficiency of the trigger in that H_{T} bin. The α_{T} thresholds of the `HTxxx_AlphaT0pyy` triggers were tuned according to the threshold on the H_{T} leg in order to fully suppress QCD multijet events and simultaneously satisfying other criteria, such as maintaining acceptable trigger rates.

The `HTxxx_AlphaT0pyy` trigger efficiencies are measured with a reference (i.e., unbiased) event sample recorded by an unprescaled, loosely-isolated, eta-restricted single muon trigger, `HLT_IsoMu24_eta2p1`, within the `SingleMu` dataset. A sample of events containing at least one isolated muon with $p_{\mathrm{T}} > 25\,\mathrm{GeV}$ and $|\eta| < 2.1$ is used (similar to the μ + jets control sample defined in Section **??**). A cut of $\Delta\mathrm{R} > 0.5$ is placed between all muons and jets in each event, and only jets are considered in the calculation of H_{T}, $\not{H}_{\mathrm{T}}$, and α_{T}, i.e. the muon is ignored.

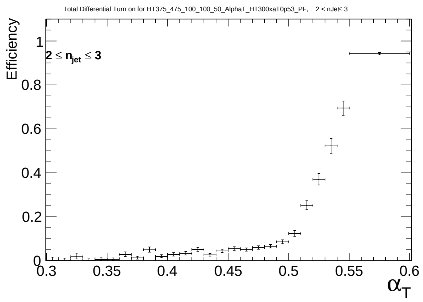

(a) Differential, $375 < H_{\mathrm{T}} < 475\,\mathrm{GeV}$

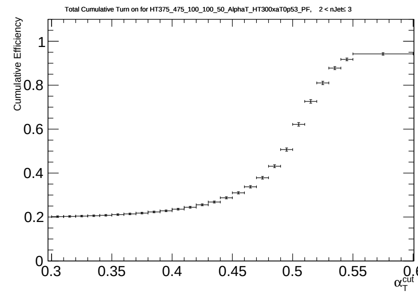

(b) Cumulative, $375 < H_{\mathrm{T}} < 475\,\mathrm{GeV}$

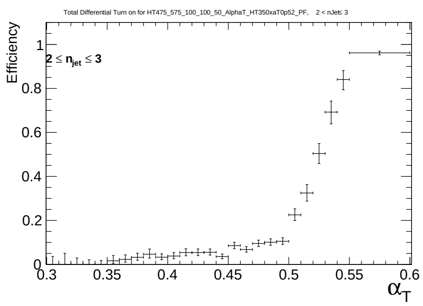

(c) Differential, $475 < H_{\mathrm{T}} < 525\,\mathrm{GeV}$

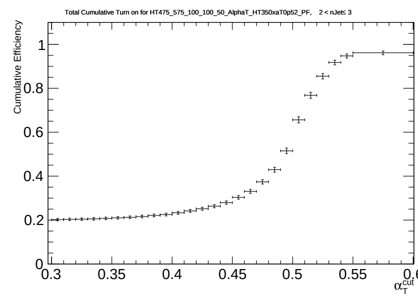

(d) Cumulative, $475 < H_{\mathrm{T}} < 525\,\mathrm{GeV}$

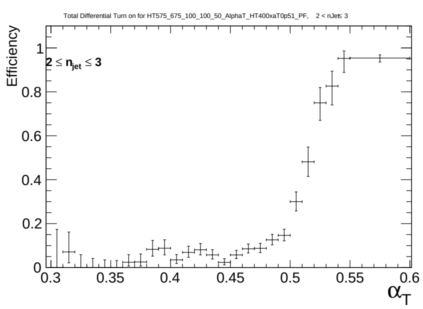

(e) Differential, $525 < H_{\mathrm{T}} < 675\,\mathrm{GeV}$

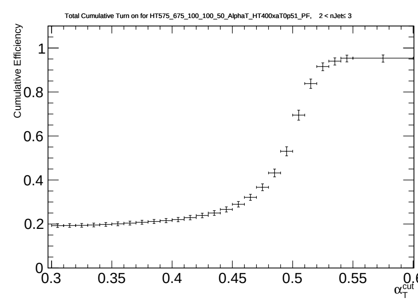

(f) Cumulative, $525 < H_{\mathrm{T}} < 675\,\mathrm{GeV}$

Figure 2: (Left) Differential and (Right) cumulative efficiency turn-on curves for the H_{T}-α_{T} cross triggers (as summarised in Table **??**) that record events for the three lowest H_{T} bins for events satisfying $2 \leq n_{\mathrm{jet}} \leq 3$.

Muon control samples

0.5.4 event selection

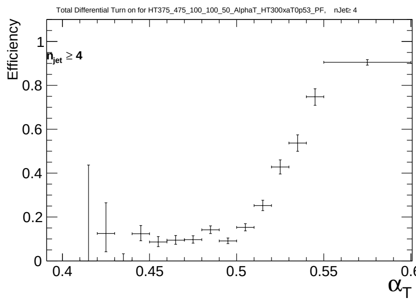

(a) Differential, $375 < H_\mathrm{T} < 475\,\mathrm{GeV}$

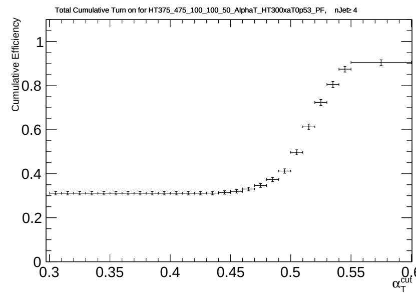

(b) Cumulative, $375 < H_\mathrm{T} < 475\,\mathrm{GeV}$

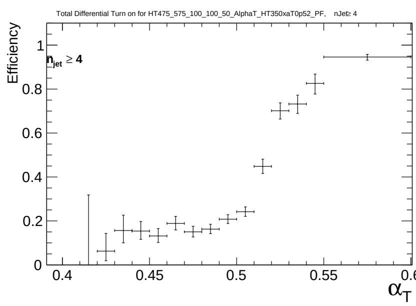

(c) Differential, $475 < H_\mathrm{T} < 525\,\mathrm{GeV}$

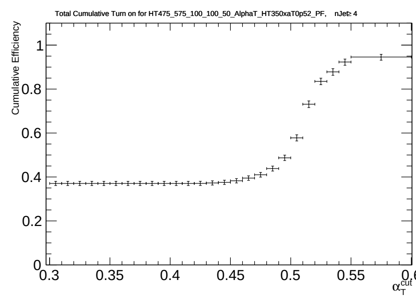

(d) Cumulative, $475 < H_\mathrm{T} < 525\,\mathrm{GeV}$

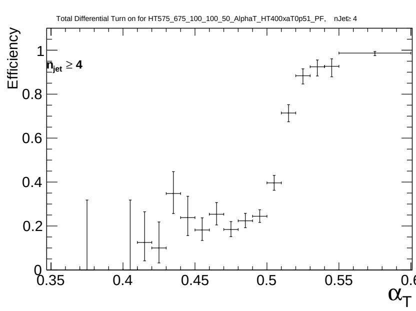

(e) Differential, $525 < H_\mathrm{T} < 675\,\mathrm{GeV}$

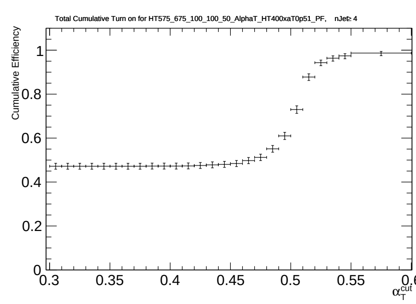

(f) Cumulative, $525 < H_\mathrm{T} < 675\,\mathrm{GeV}$

Figure 3: (Left) Differential and (Right) cumulative efficiency turn-on curves for the H_T-α_T cross triggers (as summarised in Table **??**) that record events for the three lowest H_T bins for events satisfying $n_\mathrm{jet} \geq 4$.

0.6 Closure tests and systematic uncertainties on transfer factors

Limitations in simulating detector effects and event kinematics requires us to apply appropriate systematic uncertainties on the simulation-based translation factors. The following section describes how we obtain these uncertainties through the method of closure tests.

0.6.1 Closure tests

At its core, the method compares an observed yield (N_{obs}) and a predicted yield (N_{pred}) in a subsample of a control region. The predicted yield is constructed by translating from a statistically independent data sample to the data sample of interest by the use of the proper translation factor. For example, in a given HT bin, a prediction for the $n_{\text{jet}} \geq 4$, n_{b} =1, μ + jets sample can be made by translating from the $2 \leq n_{\text{jet}} \leq 3$, n_{b} =1, μ + jets in data via the translation factor:

$$\frac{N_{\text{MC}}^{\mu+\text{jets}}(H_{\text{T}}, n_{\text{jet}} \geq 4, n_{\text{b}} = 1)}{N_{\text{MC}}^{\mu+\text{jets}}(H_{\text{T}}, 2 \leq n_{\text{jet}} \leq 3, n_{\text{b}} = 1)} \tag{1}$$

The agreement between N_{obs} and N_{pred} is expressed as $(N_{\text{obs}} - N_{\text{pred}})/N_{\text{pred}}$. Assuming only statistical uncertainties on N_{obs} and N_{pred}, deviation of the ratio from zero defines our level of closure. A closure test set is defined as ratios for each H_{T} bin. Looking at the ratio as a function of H_{T} allows the measurement of statistical significant biases from zero and/or any dependence on H_{T}. If statistically significant biases are observed, further studies are required to understand and correct for these biases.

Eight sets of closure tests probe key ingredients of the simulation modeling of the SM backgrounds with genuine $\not{E}_{\text{T}}$ as a function of H_{T}, as shown in Fig. 4. This is done for the two jet multiplicity bins separately: (a) $2 \leq n_{\text{jet}} \leq 3$ and (b) $n_{\text{jet}} \geq 4$.

Under the assumption of closure for the full ensemble of tests, systematic uncertainties on the transfer factors are derived for each n_{jet} category and H_{T} regions. The treatment for estimating the systematic uncertainties on the transfer factors is described in Section 0.6.2.

As described in section ?? The α_{T} requirement is not imposed in the μ + jets control sample. Therefore it is important to verify the approach of using μ + jets samples without an α_{T} requirement to make background predictions in the signal region. The first set of closure tests (denoted by circles) attempts to do this by probing the modeling of the α_{T} distribution in genuine $\not{E}_{\mathrm{T}}$ events as a function of H_{T}. The tests compares data yields in the μ + jets sample with an α_{T} requirement against predictions determined in a μ + jets sample with the α_{T} requirement inverted.

The next three sets (triangles, crosses, squares) probe the sensitivity of the transfer factors to the relative admixture of events from the W + jets and $t\bar{t}$ processes. These tests are conservative, since by construction, the admixture changes little when translating from the μ + jets control region to the signal region, whereas the closure tests use sub-samples with different b-tag requirements and therefore have very different admixtures of W + jets and $t\bar{t}$ events. In the $2 \leq n_{\mathrm{jet}} \leq 3$ bin, the test is sub-divided into separate jet categories. These tests also probe the modeling of the reconstruction of b-quark jets, although this also addressed more fully by dedicated studies that determine systematic uncertainties via the method described in Sec. **??**.

The remaining tests probe the simulation modeling of the jet multiplicity in the μ + jets and γ + jets samples, which is checked due to the exclusive binning in jet multiplicity. As in the case of the W + jets / $t\bar{t}$ admixture, this set of tests is a very conservative check, as predictions are always made from the same jet multiplicity bin, whereas the closure tests translate between the two bins.

Tables 4 and 5, which summarize the results obtained from fits of zeroth order polynomials (i.e. a constant) to the sets of closure tests performed in the $2 \leq n_{\mathrm{jet}} \leq 3$ and $n_{\mathrm{jet}} \geq 4$ bins. Table 6 lists the fits result common to both jet multiplicities. The best fit value and its uncertainty is listed for each set of closure tests, along with the χ^2, the number of degrees of freedom, and the p-value of the fit. The best fit value for the constant parameter is indicative of the level of closure, as averaged across the full H_{T} range considered in the analysis, and the p-value is indicative of whether there is any significant dependence on H_{T}.

The closure tests demonstrate, within the statistical precision of each test, that there are no significant biases or dependencies on H_{T} inherent in the transfer factors obtained from simulation.

One set of tests does indicate a poor goodness of fit (indicated by a low p-value), which is the $n_{\mathrm{b}} = 0 \rightarrow n_{\mathrm{b}} = 1$ test in the μ + jets sample for the $n_{\mathrm{jet}} \geq 4$ category, which has been identified as a upward (downward) fluctuation of event counts in the H_{T} bin 475–575 GeV (575–675 GeV) when $n_{\mathrm{b}} = 1$. Combining these two bins yields an acceptable fit result, as indicated in Table 5, which points to a simple fluctuation rather than any systematic bias.

Table 4: A summary of the results obtained from fits of zeroth order polynomials (i.e. a constant) to four sets of closure tests performed in the $2 \leq n_{\mathrm{jet}} \leq 3$ bin.

		Constant fit			
Closure test	Symbol	Best fit value	χ^2	d.o.f.	p-value
$\alpha_{\mathrm{T}} < 0.55 \rightarrow \alpha_{\mathrm{T}} > 0.55$ (μ + jets)	Circle	0.007 ± 0.02	3.91	7	0.79
1 b-tags $\rightarrow$2 b-tags (μ + jets, nJet=3)	Triangle	-0.008 ± 0.04	3.20	7	0.87
0 b-tags $\rightarrow$1 b-tags (μ + jets, nJet=2)	Cross	0.111 ± 0.03	5.87	7	0.55
0 b-tags $\rightarrow$1 b-tags (μ + jets, nJet=3)	Square	0.040 ± 0.02	1.12	7	0.99

Table 5: A summary of the results obtained from fits of zeroth order polynomials (i.e. a constant) to three sets of closure tests performed in the $n_{\mathrm{jet}} \geq 4$ bin. †Further explanation of this fit can be found in the text.

		Constant fit			
Closure test	Symbol	Best fit value	χ^2	d.o.f.	p-value
$\alpha_{\mathrm{T}} < 0.55 \rightarrow \alpha_{\mathrm{T}} > 0.55$ (μ + jets)	Circle	0.011 ± 0.04	5.81	7	0.56
1 b-tags $\rightarrow$2 b-tags (μ + jets)	Triangle	0.045 ± 0.03	9.36	7	0.23
0 b-tags $\rightarrow$1 b-tags (μ + jets)	Square	0.007 ± 0.03	25.30	7	0.00
0 b-tags $\rightarrow$1 b-tags (μ + jets)†	Square	0.009 ± 0.03	10.12	6	0.12

Table 6: A summary of the results obtained from fits of zeroth order polynomials (i.e. a constant) to four sets of closure tests ($2 \leq n_{\rm jet} \leq 3 \rightarrow n_{\rm jet} \geq 4$) that probe the accuracy of the MC modeling of the $n_{\rm jet}$ distribution observed in data, using the three data control samples.

		Constant fit			
Closure test	Symbol	Best fit value	χ^2	d.o.f.	p-value
$2 \leq n_{\rm jet} \leq 3 \rightarrow n_{\rm jet} \geq 4$ (μ + jets, 1 b-tags)	Times	-0.053 ± 0.03	8.02	7	0.33
$2 \leq n_{\rm jet} \leq 3 \rightarrow n_{\rm jet} \geq 4$ (μ + jets, 1 b-tags)	Invert. Triangle	0.018 ± 0.04	6.23	7	0.51
$2 \leq n_{\rm jet} \leq 3 \rightarrow n_{\rm jet} \geq 4$ (μ + jets, 0 b-tags)	Star	0.034 ± 0.02	9.24	7	0.24
$2 \leq n_{\rm jet} \leq 3 \rightarrow n_{\rm jet} \geq 4$ (γ + jets, 0 b-tags)	Diamond	0.100 ± 0.04	12.20	7	0.09

0.6.2 Systematic uncertainties from closure tests and Trigger

Once it is established that no significantly large bias or trend is observed for any set of closure tests, then systematic uncertainties are determined.

Systematics are determined for each $H_{\rm T}$ bin, as indicated in Table 7. For each $H_{\rm T}$ region, the systematic uncertainty is estimated by taking the quadrature sum of the weighted mean and sample variance for the closure tests within the given $H_{\rm T}$ region. This procedure yields the values quoted in Table 7.

As the closure tests do not translate from control region to signal region, they do not probe the uncertainty in the signal trigger efficiencies. To account for this, a trigger uncertainty of 5% is added in quadrature to the uncertainty values obtained via the closure tests and the total is summarized in Table 8.

Table 7: A summary of the magnitude of the systematic uncertainties (%) obtain from closure tests, according to $n_{\rm jet}$ and $H_{\rm T}$ region.

	$H_{\rm T}$ region (GeV)							
$n_{\rm jet}$	375–475	475–525	525–675	675–775	775–875	875-975	1075-1075	> 1175
2–3	3	4	5	11	11	16	16	16
$\geq$4	3	4	6	13	13	13	13	20

Figure 4 shows the sets of closure tests overlaid on top of gray bands that represent the $H_{\rm T}$-

Table 8: A summary of the magnitude of the total systematic uncertainties (%) assigned to the transfer factors, according to n_{jet} and H_{T} region.

	H_{T} region (GeV)							
n_{jet}	375–475	475–525	525–675	675–775	775–875	875-975	1075-1075	> 1175
2–3	6	6	7	12	12	17	17	17
$\geq$4	6	6	8	14	14	14	14	21

dependent systematic uncertainties in Table 7. These systematic uncertainties are assumed to fully uncorrelated between the different b jet multiplicity categories and also the eight H_{T} regions, which is a conservative approach given that one can expect some correlation between adjacent H_{T} bins (due to comparable kinematics).

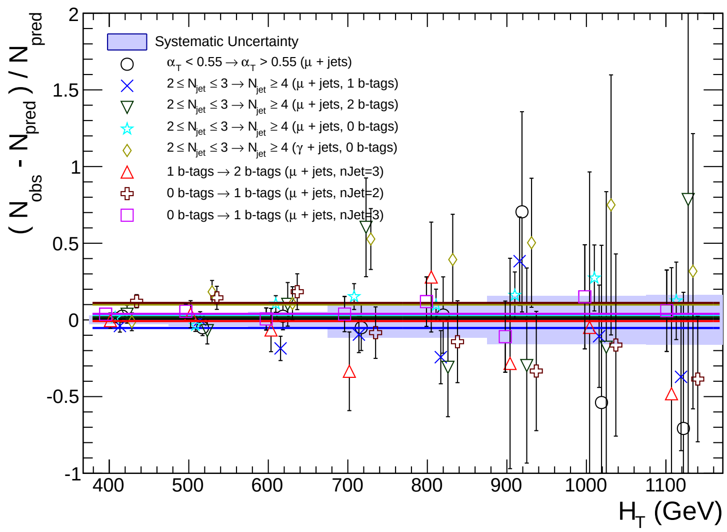

(a) $2 \leq n_{\text{jet}} \leq 3$

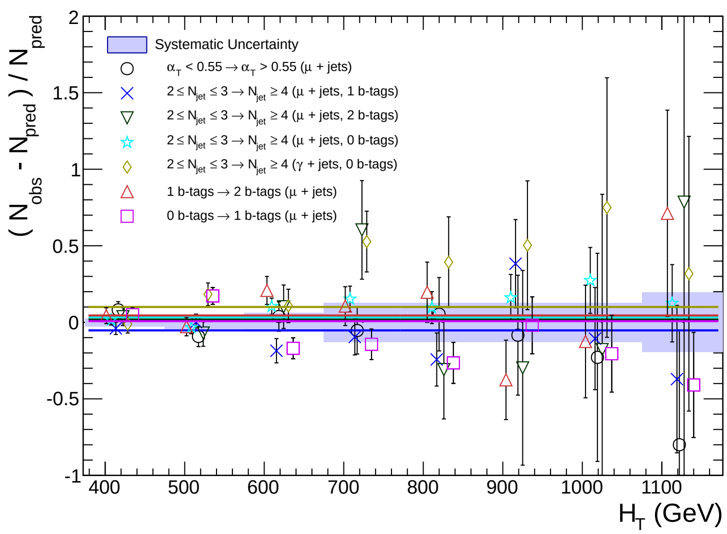

(b) $n_{\text{jet}} \geq 4$

Figure 4: Sets of closure tests (open symbols) overlaid on top of the systematic uncertainty used for each of the H_{T} region (shaded bands) and for the two different jet multiplicity bins: (a) $2 \leq n_{\text{jet}} \leq 3$ and (b) $n_{\text{jet}} \geq 4$.

0.7 Results

The likelihood described in ref:likelihood is used to relate yields, uncertainties. It is constructed using ROOTFIT [**?**] and maximized using MINUIT [**?**].

0.7.1 Standard Model

To test compatiblity with a Standard Model only hypothesis, the signal term is removed from the likelihood model. The parameter values maximizing the likelihood function are listed in Tables 11–16 found in Appendix .1. The resulting SM yields along with the observed data yields are summarized in Tables .2. The uncertainty on the yields are obtained by constructing a probability density function (p.d.f) from the maximized likelihood, then generating an ensemble of peudo-experiments from this p.d.f. and maxmizing the same likelihood form for each pseudo-experiment, resulting in an esemble of yields. The 68% quantile of each ensemeble defines the quoted uncertainty on the corresponding yield.

Figures 6–11 show the H_{T}-binned observed data yields (black filled circles) and the SM expectations and uncertainties (dark blue solid line with light blue bands) as determined by the fit for the hadronic signal region and the μ + jets or both (μ + jets,γ + jets) control samples, depending on the event category. The uncertainties in the SM expectations obtained from the ensemble of pseudo-experiments reflect the statistical uncertainties in the considered data samples and the systematic uncertainties in the transfer factors as discused in section 0.6. Figures 6–11 are summarized in tabular format in Tables 17–22 in appendix .2 along with observed data yields and the fit result for all event categories and both signal region and control sample bins.

For each n_{b}, n_{jet} category, the goodness-of-fit of the SM-only hypothesis is determined by considering simultaneously all H_{T} bins entering the likelihood. The goodness-of-fit described in [**?**] is obtained by comparing the nominal maximized likelihood value $L_{\mathrm{max}}^{\mathrm{data}}$ to the corresponding ensemble of values, L_{max}. The quantile which $L_{\mathrm{max}}^{\mathrm{data}}$ falls in the distributions is interpreted as a p-value. A p-value derived from a chi-square is also plotted for comparison.

The p-values obtained, shown in Figure 5 (Left), are found to be uniformly distributed in the range 0.0–1.0, with the lowest p-value determined to be 0.17.

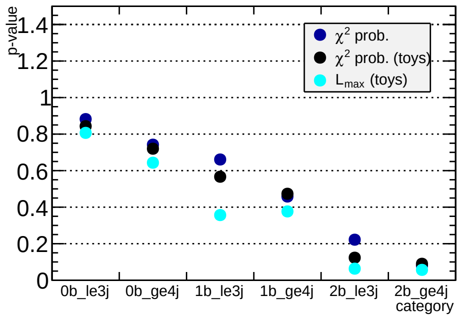

(a) p-values per event category.

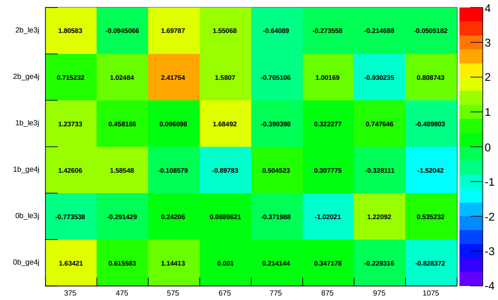

(b) Pull versus signal region bin.

Figure 5: Pulls and p-values. See text for details

Table 9: Summary of hadronic yields from fit.

	375–475	475–575	575–675	675–775	775–875	875–975	975–1075	1075–∞
0b le3j SM	2744^{+48}_{-43}	771^{+21}_{-23}	254^{+13}_{-13}	$76.5^{+6.1}_{-4.8}$	$33.7^{+3.7}_{-3.8}$	$11.8^{+1.9}_{-2.1}$	$6.3^{+1.4}_{-1.3}$	$3.2^{+1.0}_{-0.9}$
0b le3j Data	2728	766	257	77	32	9	9	4
1b le3j SM	426^{+15}_{-17}	114^{+6}_{-6}	$35.5^{+3.3}_{-2.8}$	$10.1^{+1.4}_{-1.5}$	$3.7^{+0.9}_{-0.8}$	$1.6^{+0.7}_{-0.6}$	$0.5^{+0.3}_{-0.4}$	$0.1^{+0.1}_{-0.0}$
1b le3j Data	444	118	36	15	3	2	1	0
2b le3j SM	$65.0^{+4.3}_{-4.3}$	$18.4^{+1.7}_{-1.6}$	$4.2^{+0.6}_{-0.5}$	$1.1^{+0.3}_{-0.2}$	$0.2^{+0.1}_{-0.1}$	$0.0^{+0.0}_{-0.0}$	$0.0^{+0.0}_{-0.0}$	$0.0^{+0.0}_{-0.0}$
2b le3j Data	78	18	8	3	0	0	0	0
0b ge4j SM	456^{+15}_{-14}	291^{+12}_{-12}	148^{+8}_{-7}	$66.0^{+5.6}_{-5.2}$	$27.1^{+2.9}_{-3.4}$	$14.0^{+1.9}_{-2.1}$	$6.5^{+1.5}_{-1.2}$	$3.2^{+1.0}_{-0.9}$
0b ge4j Data	480	299	158	66	28	15	6	2
1b ge4j SM	190^{+10}_{-8}	120^{+6}_{-5}	$45.6^{+3.1}_{-3.8}$	$17.1^{+2.6}_{-1.9}$	$6.8^{+1.5}_{-1.3}$	$5.4^{+1.3}_{-1.6}$	$2.4^{+0.9}_{-0.9}$	$1.2^{+0.7}_{-0.8}$
1b ge4j Data	206	135	45	14	8	6	2	0
2b ge4j SM	$73.6^{+4.2}_{-4.2}$	$45.7^{+2.8}_{-2.9}$	$20.4^{+1.8}_{-1.8}$	$7.7^{+1.2}_{-1.0}$	$1.9^{+0.3}_{-0.3}$	$0.9^{+0.2}_{-0.2}$	$0.4^{+0.1}_{-0.1}$	$0.4^{+0.1}_{-0.2}$
2b ge4j Data	79	52	31	12	1	2	0	1

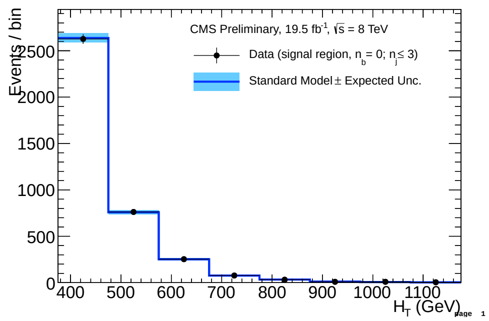

(a) Hadronic sample (linear scale)

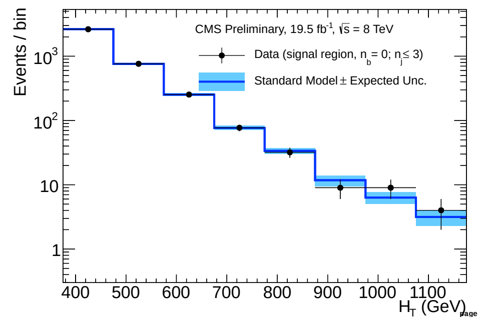

(b) Hadronic sample (logarithmic scale)

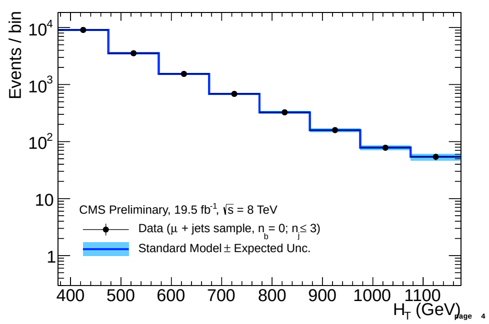

(c) μ + jets sample

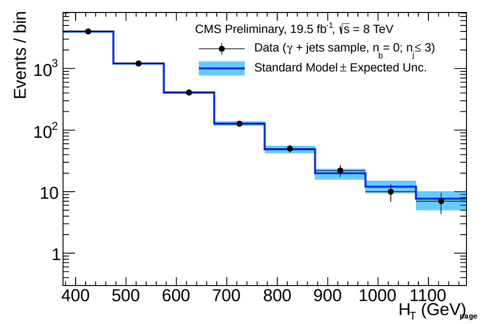

(d) γ + jets sample

Figure 6: Comparison of the H_{T}-binned observed data yields and SM expectations when requiring $2 \leq n_{\mathrm{jet}} \leq 3$ and $n_{\mathrm{b}} = 0$ for the (a-b) hadronic, (c) μ + jets, (d) $\mu\mu$ + jets and (e) γ + jets samples, as determined by a simultaneous fit to all data samples under the SM-only hypothesis. The observed event yields in data (black dots) and the expectations and their uncertainties (dark blue solid line with light blue bands), as determined by the simultaneous fit, are shown. For illustrative purposes only, the signal expectations (pink dashed line) for the model T2cc with $m_{\tilde{\mathrm{q}}} = 250\,\mathrm{GeV}$ and $m_{\mathrm{LSP}} = 240\,\mathrm{GeV}$ are stacked on top of the SM expectations.

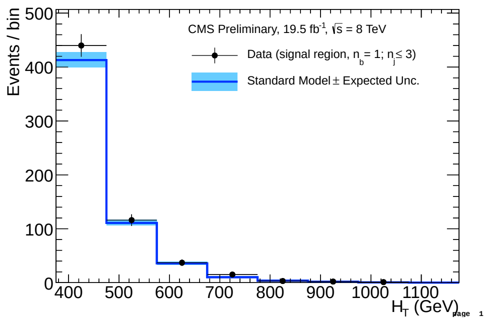

(a) Hadronic sample (linear scale)

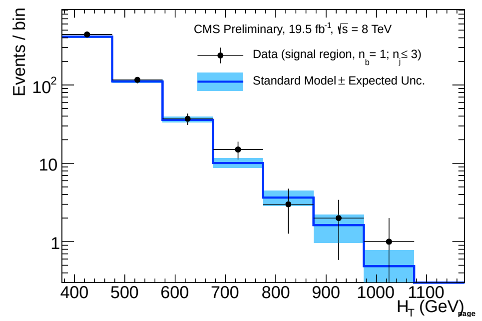

(b) Hadronic sample (logarithmic scale)

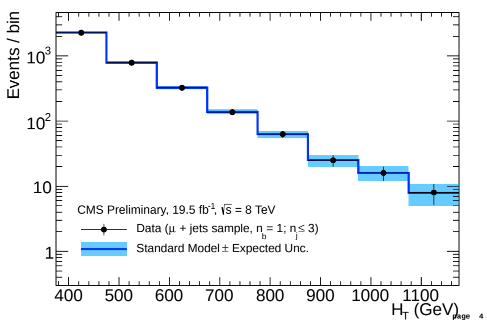

(c) μ + jets sample

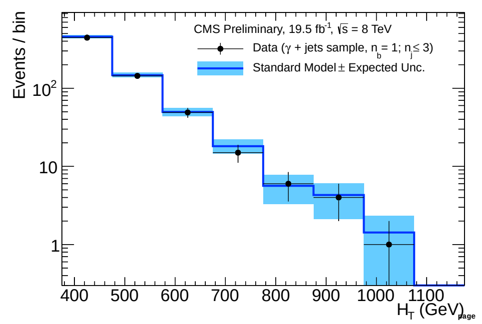

(d) γ + jets sample

Figure 7: Comparison of the H_{T}-binned observed data yields and SM expectations when requiring $2 \leq n_{\mathrm{jet}} \leq 3$ and $n_{\mathrm{b}} = 1$ for the (a-b) hadronic, (c) μ + jets, (d) $\mu\mu$ + jets and (e) γ + jets samples, as determined by a simultaneous fit to all data samples under the SM-only hypothesis. The observed event yields in data (black dots) and the expectations and their uncertainties (dark blue solid line with light blue bands), as determined by the simultaneous fit, are shown. For illustrative purposes only, the signal expectations (pink dashed line) for the model `T2cc` with $m_{\tilde{\mathrm{q}}} = 250\,\mathrm{GeV}$ and $m_{\mathrm{LSP}} = 170\,\mathrm{GeV}$ are stacked on top of the SM expectations.

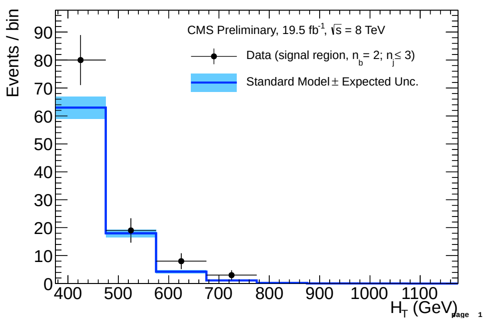

(a) Hadronic sample (linear scale)

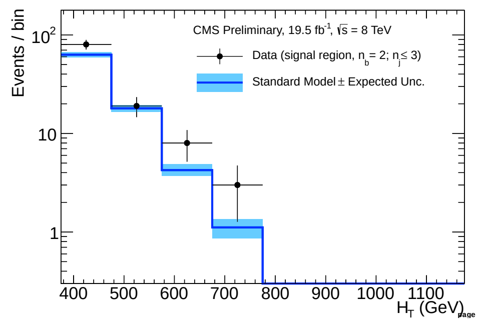

(b) Hadronic sample (logarithmic scale)

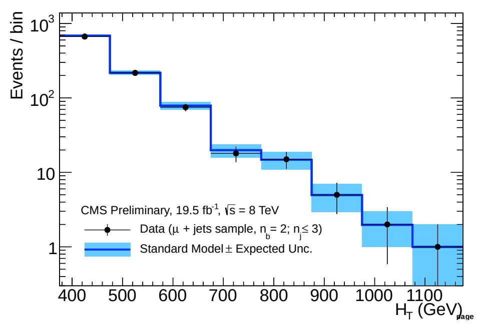

(c) μ + jets sample

Figure 8: Comparison of the H_{T}-binned observed data yields and SM expectations when requiring $2 \leq n_{\mathrm{jet}} \leq 3$ and $n_{\mathrm{b}} = 2$ for the (a-b) hadronic and μ + jets samples, as determined by a simultaneous fit to both the hadronic and μ + jets data samples under the SM-only hypothesis. The observed event yields in data (black dots) and the expectations and their uncertainties (dark blue solid line with light blue bands), as determined by the simultaneous fit, are shown.

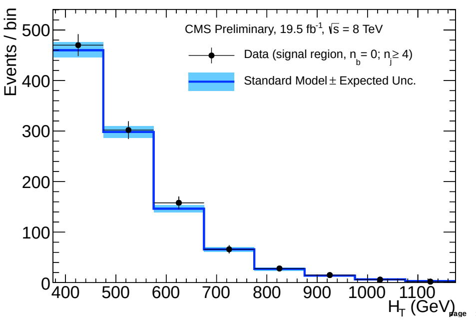

(a) Hadronic sample (linear scale)

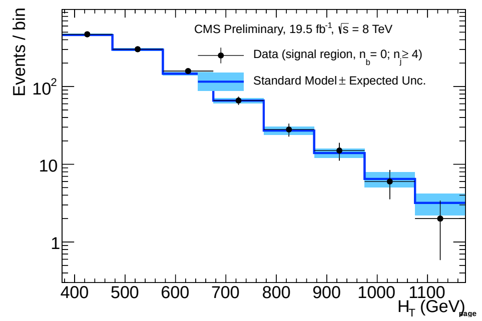

(b) Hadronic sample (logarithmic scale)

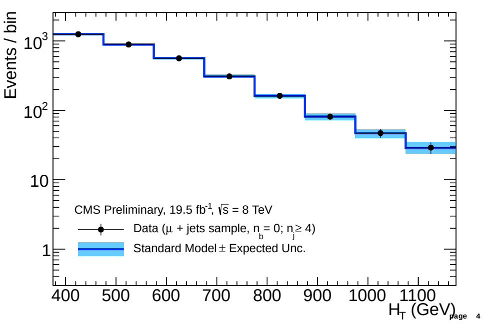

(c) μ + jets sample

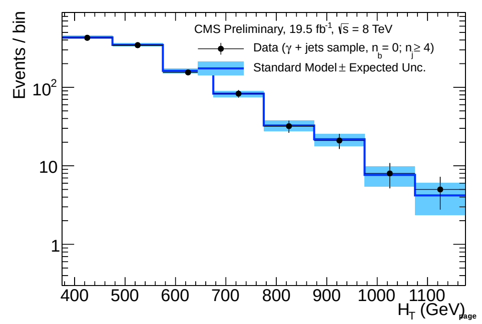

(d) γ + jets sample

Figure 9: Comparison of the H_T-binned observed data yields and SM expectations when requiring $n_{\text{jet}} \geq 4$ and $n_b = 0$ for the (a-b) hadronic, (c) μ + jets, (d) $\mu\mu$ + jets and (e) γ + jets samples, as determined by a simultaneous fit to all data samples under the SM-only hypothesis. The observed event yields in data (black dots) and the expectations and their uncertainties (dark blue solid line with light blue bands), as determined by the simultaneous fit, are shown. For illustrative purposes only, the signal expectations (pink dashed line) for the model `T2cc` with $m_{\tilde{q}} = 250\,\text{GeV}$ and $m_{\text{LSP}} = 170\,\text{GeV}$ are stacked on top of the SM expectations.

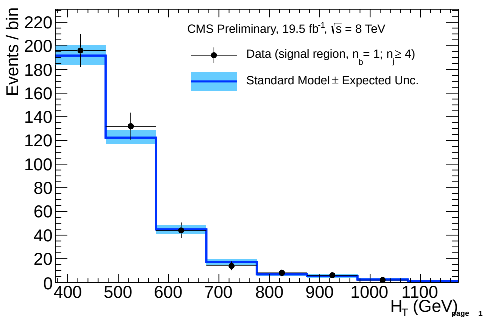

(a) Hadronic sample (linear scale)

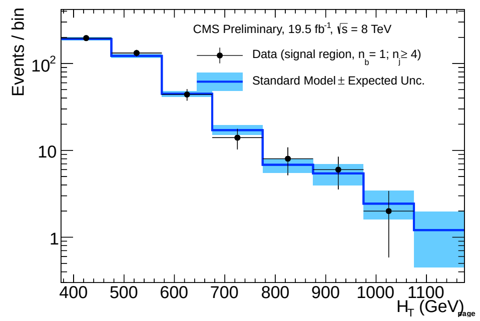

(b) Hadronic sample (logarithmic scale)

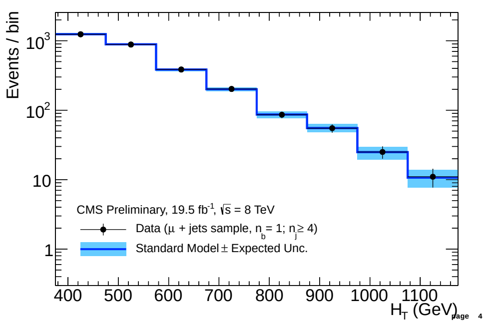

(c) μ + jets sample

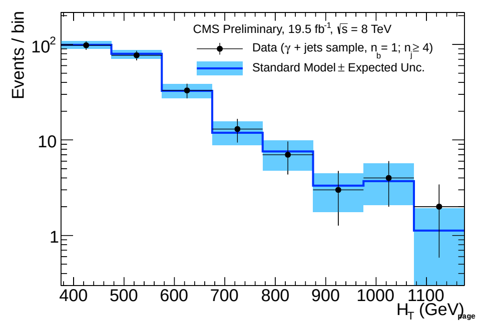

(d) γ + jets sample

Figure 10: Comparison of the H_{T}-binned observed data yields and SM expectations when requiring $n_{\text{jet}} \geq 4$ and $n_{\mathrm{b}} = 1$ for the (a-b) hadronic, (c) μ + jets, (d) $\mu\mu$ + jets and (e) γ + jets samples, as determined by a simultaneous fit to all data samples under the SM-only hypothesis. The observed event yields in data (black dots) and the expectations and their uncertainties (dark blue solid line with light blue bands), as determined by the simultaneous fit, are shown. For illustrative purposes only, the signal expectations (pink dashed line) for the model T2cc with $m_{\tilde{\mathrm{q}}} = 250\,\mathrm{GeV}$ and $m_{\mathrm{LSP}} = 170\,\mathrm{GeV}$ are stacked on top of the SM expectations.

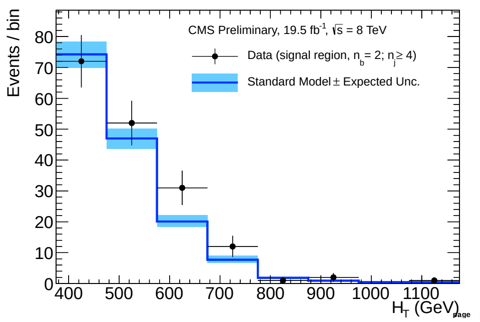

(a) Hadronic sample (linear scale)

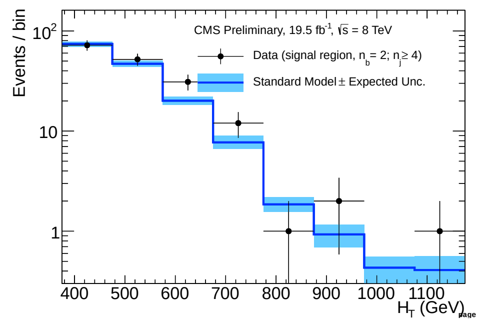

(b) Hadronic sample (logarithmic scale)

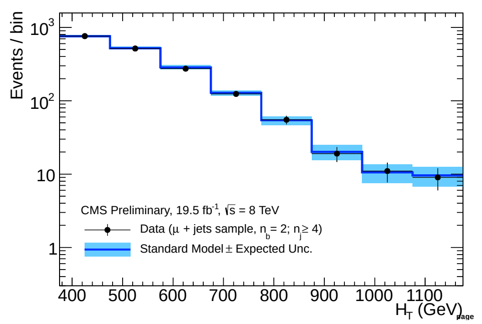

(c) μ + jets sample

Figure 11: Comparison of the H_{T}-binned observed data yields and SM expectations when requiring $n_{\mathrm{jet}} \geq 4$ and $n_{\mathrm{b}} = 2$ for the (a-b) hadronic and μ + jets samples, as determined by a simultaneous fit to both the hadronic and μ + jets data samples under the SM-only hypothesis. The observed event yields in data (black dots) and the expectations and their uncertainties (dark blue solid line with light blue bands), as determined by the simultaneous fit, are shown.

0.8 Signal models and efficiencies

fill

0.8.1 Introduction

As mentioned in section **??**, SUSY is a theory of many particles and parameters. Simplifed models (SMS) have been derived [**? ? ?**] which reduce both particles and parameters at the cost of losing generality of the full SUSY model. Yet, SMS models are benificial experimentally, as they provide clear signatures to search for. Two SMS models have been studied 1. T2cc: pair produced stop sparticles each decaying into a charm quark and a neutralino. 2. T2tt: pair produced stop sparticles each decaying into a top quart and a neutralino.

Event samples for the simplified models are generated by the CMS SUSY MC group [REF] at leading order with MadGraph [**?**]. Inclusive, process-dependent, next-to-leading order calculations with next-to-leading logarithmic corrections [**?**] (NLO+NLL) of SUSY production cross sections are obtained with the program PROSPINO [**?**] and `CTEQ6L` [**?**] parton distribution functions. The `FastSim` framework is used, and the simulated signal events include multiple interactions per LHC bunch crossing (pileup) with the distribution of reconstructed vertices that match the one observed in data. The MC samples are listed in Section 0.4.

The SMS samples are produced in bins of stop mass (mStop) and neutralino mass (mLSP). The analysis efficieny is studied in the usual n_{jet}, n_{b} binning but due to computational limitations not all categories are used to set a limit on a given model. The choice of categories for a model is made by computing the expected upper limit on the signal cross-section for each category seperatly using the much quicker asymptotic method [REF]. The categories are ranked by their expected upper limit. Depending on the number of mass bins and number of events per bin, two or more categories with the higest rank are chosen.

The simplified models, along with the event categories considered for each, is summarised in

Table 10.

Table 10: A summary of the simplified models considered for interpretation. The event categories considered for each model are listed.

Model	Production/decay mode	($n_{\rm jet}$,$n_{\rm b}$) event categories considered
T2cc	pp $\rightarrow \tilde{t}\tilde{t}^{*} \rightarrow$ c$\tilde{\chi}^{0}$ $\bar{\rm c}\tilde{\chi}^{0}$	(2–3,0), ($\geq$ 4,0), ($\geq$ 4,1)
T2tt	pp $\rightarrow \tilde{t}\tilde{t}^{*} \rightarrow$ t$\tilde{\chi}^{0}$ $\bar{\rm t}\tilde{\chi}^{0}$	($\leq$ 3,1), ($\leq$ 4,2)

0.8.2 Efficiency times acceptance for T2cc

Figure 12 (Appendix .3.1) shows the expected signal efficiency times acceptance for the signal region and μ + jets control sample (i.e., signal contamination) for the model T2cc in the four most sensitive ($n_{\rm jet}$,$n_{\rm b}$) event categories: (2–3,0), (2–3,1), ($\geq$ 4,0), and ($\geq$ 4,1). The choice of which categories to use is made by inspecting Figure **??** (Appendix .3.1), which shows the expected significance per signal region bin following the injection of signal at the theoretical QCD production cross section for the T2cc model mass points $m_{\tilde{t}}$ = 250 GeV and $m_{\rm LSP}$ = 170 GeV (Top) and $m_{\rm LSP}$ = 240 GeV (Bottom).

The efficiencies are typically at the percent level or less due to reliance on hard-$p_{\rm T}$ jets from initial state radiation for acceptance in the presence of a compressed mass spectrum and soft decay products. The largest efficiencies for the smallest mass splittings, $\Delta M =\sim 10$ GeV, are obtained with the (2–3,0) category, while for larger mass splittings the (2–3,1), ($\geq$ 4,0), and ($\geq$ 4,1) categories contribute due to the reduced backgrounds in these categories. The signal efficiency in the μ + jets control sample is negligible with respect to the signal region. By extension, the relative contamination for the $\mu\mu$ + jets sample is also considered to be negligible. Regardless, any potential contamination is accounted for in the likelihood model.

.1 Maximum likelihood parameter values

Table 11: SM-only maximum-likelihood parameter values (0b le3j).

name	value	error
EWK^0	2.64e+03	4.7e+01
EWK^1	7.59e+02	2.2e+01
EWK^2	2.52e+02	1.1e+01
EWK^3	7.64e+01	6.0e+00
EWK^4	3.37e+01	3.5e+00
EWK^5	1.18e+01	2.0e+00
EWK^6	6.32e+00	1.4e+00
EWK^7	3.15e+00	8.9e-01
f^0_{Zinv}	0.64	0.02
f^1_{Zinv}	0.67	0.02
f^2_{Zinv}	0.70	0.02
f^3_{Zinv}	0.70	0.04
f^4_{Zinv}	0.69	0.04
f^5_{Zinv}	0.76	0.05
f^6_{Zinv}	0.76	0.06
f^7_{Zinv}	0.82	0.06
$\rho^0_{\mu W}$	1.01	0.05
$\rho^1_{\mu W}$	1.00	0.06
$\rho^2_{\mu W}$	1.00	0.07
$\rho^3_{\mu W}$	1.00	0.11
$\rho^4_{\mu W}$	1.01	0.11
$\rho^5_{\mu W}$	1.02	0.16
$\rho^6_{\mu W}$	0.98	0.15
$\rho^7_{\mu W}$	1.00	0.16
$\rho^0_{\gamma Z}$	1.02	0.04
$\rho^1_{\gamma Z}$	0.99	0.04
$\rho^2_{\gamma Z}$	1.00	0.06
$\rho^3_{\gamma Z}$	0.99	0.10
$\rho^4_{\gamma Z}$	1.02	0.11
$\rho^5_{\gamma Z}$	1.05	0.16
$\rho^6_{\gamma Z}$	0.95	0.14
$\rho^7_{\gamma Z}$	0.98	0.15

Table 12: SM-only maximum-likelihood parameter values (1b le3j).

name	value	error
EWK^0	4.13e+02	1.4e+01
EWK^1	1.11e+02	5.9e+00
EWK^2	3.58e+01	3.0e+00
EWK^3	1.01e+01	1.6e+00
EWK^4	3.66e+00	8.2e-01
EWK^5	1.63e+00	6.0e-01
EWK^6	4.87e-01	3.1e-01
EWK^7	1.21e-01	4.7e-02
f^0_{Zinv}	0.47	0.02
f^1_{Zinv}	0.55	0.03
f^2_{Zinv}	0.57	0.04
f^3_{Zinv}	0.64	0.07
f^4_{Zinv}	0.55	0.11
f^5_{Zinv}	0.81	0.08
f^6_{Zinv}	0.82	0.12
f^7_{Zinv}	0.00	0.83
$\rho^0_{\mu W}$	0.95	0.05
$\rho^1_{\mu W}$	0.99	0.06
$\rho^2_{\mu W}$	1.00	0.07
$\rho^3_{\mu W}$	0.98	0.11
$\rho^4_{\mu W}$	1.00	0.11
$\rho^5_{\mu W}$	1.00	0.16
$\rho^6_{\mu W}$	1.00	0.16
$\rho^7_{\mu W}$	1.00	0.16
$\rho^0_{\gamma Z}$	0.96	0.05
$\rho^1_{\gamma Z}$	0.99	0.06
$\rho^2_{\gamma Z}$	1.00	0.07
$\rho^3_{\gamma Z}$	0.96	0.11
$\rho^4_{\gamma Z}$	1.00	0.11
$\rho^5_{\gamma Z}$	0.99	0.15
$\rho^6_{\gamma Z}$	0.99	0.15
$\rho^7_{\gamma Z}$	1.00	0.16

Table 13: SM-only maximum-likelihood parameter values (2b le3j).

name	value	error
EWK^0	6.30e+01	3.8e+00
EWK^1	1.80e+01	1.5e+00
EWK^2	4.25e+00	5.4e-01
EWK^3	1.11e+00	2.7e-01
EWK^4	2.10e-01	5.9e-02
EWK^5	3.83e-02	1.8e-02
EWK^6	2.33e-02	1.7e-02
EWK^7	1.30e-03	1.3e-03
$\rho^0_{\mu W}$	0.94	0.05
$\rho^1_{\mu W}$	1.00	0.06
$\rho^2_{\mu W}$	0.98	0.07
$\rho^3_{\mu W}$	0.98	0.11
$\rho^4_{\mu W}$	1.00	0.11
$\rho^5_{\mu W}$	1.00	0.16
$\rho^6_{\mu W}$	1.00	0.16
$\rho^7_{\mu W}$	1.00	0.16

Table 14: SM-only maximum-likelihood parameter values (0b ge4j).

name	value	error
EWK^0	4.60e+02	1.6e+01
EWK^1	2.98e+02	1.2e+01
EWK^2	1.46e+02	8.2e+00
EWK^3	6.59e+01	5.7e+00
EWK^4	2.71e+01	3.3e+00
EWK^5	1.39e+01	2.2e+00
EWK^6	6.47e+00	1.5e+00
EWK^7	3.19e+00	9.5e-01
f^0_{Zinv}	0.52	0.02
f^1_{Zinv}	0.60	0.02
f^2_{Zinv}	0.61	0.03
f^3_{Zinv}	0.63	0.05
f^4_{Zinv}	0.71	0.05
f^5_{Zinv}	0.73	0.06
f^6_{Zinv}	0.74	0.07
f^7_{Zinv}	0.67	0.11
$\rho^0_{\mu W}$	0.98	0.05
$\rho^1_{\mu W}$	1.00	0.06
$\rho^2_{\mu W}$	0.97	0.07
$\rho^3_{\mu W}$	1.00	0.13
$\rho^4_{\mu W}$	1.00	0.13
$\rho^5_{\mu W}$	1.00	0.13
$\rho^6_{\mu W}$	1.00	0.13
$\rho^7_{\mu W}$	1.01	0.19
$\rho^0_{\gamma Z}$	0.98	0.05
$\rho^1_{\gamma Z}$	0.99	0.05
$\rho^2_{\gamma Z}$	0.96	0.07
$\rho^3_{\gamma Z}$	1.00	0.11
$\rho^4_{\gamma Z}$	0.99	0.12
$\rho^5_{\gamma Z}$	0.99	0.12
$\rho^6_{\gamma Z}$	1.01	0.13
$\rho^7_{\gamma Z}$	1.03	0.19

Table 15: SM-only maximum-likelihood parameter values (1b ge4j).

name	value	error
EWK^0	1.92e+02	8.5e+00
EWK^1	1.22e+02	6.1e+00
EWK^2	4.48e+01	3.5e+00
EWK^3	1.71e+01	2.1e+00
EWK^4	6.82e+00	1.3e+00
EWK^5	5.43e+00	1.5e+00
EWK^6	2.43e+00	7.9e-01
EWK^7	1.21e+00	6.3e-01
f^0_{Zinv}	0.23	0.02
f^1_{Zinv}	0.29	0.03
f^2_{Zinv}	0.38	0.05
f^3_{Zinv}	0.36	0.08
f^4_{Zinv}	0.49	0.10
f^5_{Zinv}	0.58	0.12
f^6_{Zinv}	0.70	0.11
f^7_{Zinv}	0.72	0.16
$\rho^0_{\mu W}$	0.99	0.05
$\rho^1_{\mu W}$	0.98	0.05
$\rho^2_{\mu W}$	1.00	0.07
$\rho^3_{\mu W}$	1.03	0.13
$\rho^4_{\mu W}$	0.99	0.13
$\rho^5_{\mu W}$	1.00	0.13
$\rho^6_{\mu W}$	1.00	0.13
$\rho^7_{\mu W}$	1.01	0.19
$\rho^0_{\gamma Z}$	1.00	0.06
$\rho^1_{\gamma Z}$	0.99	0.06
$\rho^2_{\gamma Z}$	1.00	0.08
$\rho^3_{\gamma Z}$	1.02	0.13
$\rho^4_{\gamma Z}$	0.99	0.13
$\rho^5_{\gamma Z}$	0.99	0.13
$\rho^6_{\gamma Z}$	1.01	0.13
$\rho^7_{\gamma Z}$	1.03	0.19

Table 16: SM-only maximum-likelihood parameter values (2b ge4j).

name	value	error
EWK^0	7.42e+01	4.4e+00
EWK^1	4.70e+01	3.1e+00
EWK^2	2.01e+01	1.8e+00
EWK^3	7.71e+00	1.1e+00
EWK^4	1.85e+00	3.4e-01
EWK^5	9.29e-01	2.3e-01
EWK^6	4.32e-01	1.4e-01
EWK^7	4.09e-01	1.5e-01
$\rho^0_{\mu W}$	1.01	0.05
$\rho^1_{\mu W}$	0.98	0.05
$\rho^2_{\mu W}$	0.94	0.07
$\rho^3_{\mu W}$	0.93	0.11
$\rho^4_{\mu W}$	1.01	0.13
$\rho^5_{\mu W}$	0.98	0.13
$\rho^6_{\mu W}$	1.01	0.13
$\rho^7_{\mu W}$	0.98	0.18

.2 SM-only yield tables

The following tables compare the observations in the hadronic and control samples with the maximum-likelihood expectations obtained by the SM-only fit.

Table 17: 0b le3j

H_T Bin (GeV)	375–475	475–575	575–675	675–775	775–875	875–975	975–1075	1075–∞
SM hadronic	2744^{+48}_{-43}	771^{+21}_{-23}	254^{+13}_{-13}	$76.5^{+6.1}_{-4.8}$	$33.7^{+3.7}_{-3.8}$	$11.8^{+1.9}_{-2.1}$	$6.3^{+1.4}_{-1.3}$	$3.2^{+1.0}_{-0.9}$
Data hadronic	2728	766	257	77	32	9	9	4
SM μ+jets	9072^{+97}_{-113}	3543^{+56}_{-62}	1539^{+39}_{-41}	686^{+25}_{-26}	325^{+17}_{-17}	158^{+13}_{-12}	$78.6^{+7.8}_{-8.3}$	$54.1^{+7.0}_{-6.8}$
Data μ+jets	9078	3545	1538	686	326	159	78	54
SM γ+jets	3990^{+54}_{-61}	1203^{+34}_{-37}	410^{+17}_{-19}	127^{+10}_{-10}	$48.8^{+6.0}_{-6.9}$	$19.9^{+3.3}_{-4.2}$	$12.1^{+3.0}_{-2.9}$	$7.7^{+2.9}_{-2.7}$
Data γ+jets	4000	1206	408	127	50	22	10	7

Table 18: 0b ge4j

H_T Bin (GeV)	375–475	475–575	575–675	675–775	775–875	875–975	975–1075	1075–∞
SM hadronic	456^{+15}_{-14}	291^{+12}_{-12}	148^{+8}_{-7}	$66.0^{+5.6}_{-5.2}$	$27.1^{+2.9}_{-3.4}$	$14.0^{+1.9}_{-2.1}$	$6.5^{+1.5}_{-1.2}$	$3.2^{+1.0}_{-0.9}$
Data hadronic	480	299	158	66	28	15	6	2
SM μ+jets	1260^{+36}_{-36}	891^{+29}_{-30}	566^{+23}_{-23}	308^{+20}_{-14}	162^{+11}_{-12}	$81.3^{+8.6}_{-8.1}$	$46.9^{+7.3}_{-6.1}$	$28.6^{+6.4}_{-4.4}$
Data μ+jets	1249	888	562	308	162	81	47	29
SM γ+jets	439^{+20}_{-18}	349^{+16}_{-18}	161^{+10}_{-13}	$83.0^{+7.9}_{-8.5}$	$32.6^{+5.7}_{-5.6}$	$21.8^{+3.6}_{-4.2}$	$7.7^{+2.4}_{-2.0}$	$4.2^{+1.7}_{-1.7}$
Data γ+jets	427	344	155	83	32	21	8	5

Table 19: 1b le3j

H_T Bin (GeV)	375–475	475–575	575–675	675–775	775–875	875–975	975–1075	1075–∞
SM hadronic	426^{+15}_{-17}	114^{+6}_{-6}	$35.5^{+3.3}_{-2.8}$	$10.1^{+1.4}_{-1.5}$	$3.7^{+0.9}_{-0.8}$	$1.6^{+0.7}_{-0.6}$	$0.5^{+0.3}_{-0.4}$	$0.1^{+0.1}_{-0.0}$
Data hadronic	444	118	36	15	3	2	1	0
SM μ+jets	2282^{+50}_{-45}	789^{+26}_{-27}	325^{+20}_{-17}	139^{+11}_{-14}	$62.7^{+9.2}_{-6.5}$	$25.1^{+4.8}_{-5.1}$	$16.1^{+3.9}_{-4.1}$	$7.9^{+2.9}_{-2.9}$
Data μ+jets	2272	787	325	137	63	25	16	8
SM γ+jets	452^{+20}_{-22}	146^{+9}_{-10}	$49.3^{+6.6}_{-5.9}$	$18.1^{+3.8}_{-4.4}$	$5.6^{+2.4}_{-2.4}$	$4.3^{+1.9}_{-1.8}$	$1.4^{+1.0}_{-1.4}$	$0.0^{+0.0}_{--0.0}$
Data γ+jets	444	144	49	15	6	4	1	0

Table 20: 1b ge4j

H_T Bin (GeV)	375–475	475–575	575–675	675–775	775–875	875–975	975–1075	1075–∞
SM hadronic	190^{+10}_{-8}	120^{+6}_{-5}	$45.6^{+3.1}_{-3.8}$	$17.1^{+2.6}_{-1.9}$	$6.8^{+1.5}_{-1.3}$	$5.4^{+1.3}_{-1.6}$	$2.4^{+0.9}_{-0.9}$	$1.2^{+0.7}_{-0.8}$
Data hadronic	206	135	45	14	8	6	2	0
SM μ+jets	1250^{+37}_{-28}	891^{+27}_{-31}	385^{+21}_{-20}	200^{+12}_{-12}	$86.6^{+9.0}_{-10.1}$	$55.3^{+7.7}_{-7.3}$	$24.9^{+4.4}_{-5.3}$	$10.7^{+3.1}_{-3.4}$
Data μ+jets	1238	881	385	202	86	55	25	11
SM γ+jets	102^{+10}_{-9}	$81.3^{+8.2}_{-7.9}$	$32.7^{+5.5}_{-5.6}$	$11.9^{+3.7}_{-3.0}$	$7.6^{+2.6}_{-2.6}$	$3.3^{+1.2}_{-1.6}$	$3.7^{+1.9}_{-1.9}$	$1.1^{+0.8}_{-1.1}$
Data γ+jets	98	77	33	13	7	3	4	2

Table 21: 2b le3j

H_T Bin (GeV)	375–475	475–575	575–675	675–775	775–875	875–975	975–1075	1075–∞
SM hadronic	$65.0^{+4.3}_{-4.3}$	$18.4^{+1.7}_{-1.6}$	$4.2^{+0.6}_{-0.5}$	$1.1^{+0.3}_{-0.2}$	$0.2^{+0.1}_{-0.1}$	$0.0^{+0.0}_{-0.0}$	$0.0^{+0.0}_{-0.0}$	$0.0^{+0.0}_{-0.0}$
Data hadronic	78	18	8	3	0	0	0	0
SM μ+jets	681^{+26}_{-31}	217^{+14}_{-14}	$78.8^{+9.4}_{-9.3}$	$19.9^{+4.1}_{-3.8}$	$14.8^{+4.0}_{-3.9}$	$5.0^{+2.0}_{-2.1}$	$2.0^{+1.0}_{-1.0}$	$1.0^{+1.0}_{-1.0}$
Data μ+jets	668	217	75	18	15	5	2	1
Data γ+jets	36	8	4	0	0	1	0	0

Table 22: 2b ge4j

H_T Bin (GeV)	375–475	475–575	575–675	675–775	775–875	875–975	975–1075	1075–∞
SM hadronic	$73.6^{+4.2}_{-4.2}$	$45.7^{+2.8}_{-2.9}$	$20.4^{+1.8}_{-1.8}$	$7.7^{+1.2}_{-1.0}$	$1.9^{+0.3}_{-0.3}$	$0.9^{+0.2}_{-0.2}$	$0.4^{+0.1}_{-0.1}$	$0.4^{+0.1}_{-0.2}$
Data hadronic	79	52	31	12	1	2	0	1
SM μ+jets	765^{+26}_{-27}	521^{+23}_{-22}	285^{+15}_{-17}	128^{+12}_{-10}	$54.1^{+7.5}_{-8.0}$	$20.1^{+4.6}_{-4.1}$	$10.6^{+2.9}_{-2.9}$	$9.6^{+2.9}_{-2.9}$
Data μ+jets	760	515	274	124	55	19	11	9
Data γ+jets	19	17	10	4	0	2	1	0

.3 Efficiencies and systematic uncertainties for simplified models

.3.1 T2cc

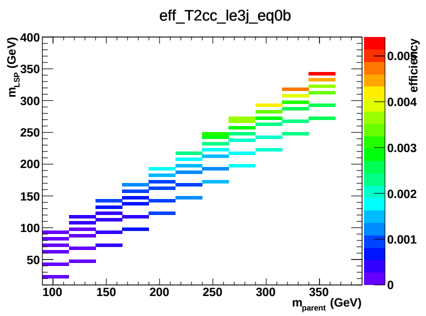

(a) Hadronic Selection Efficiency, (2–3,0)

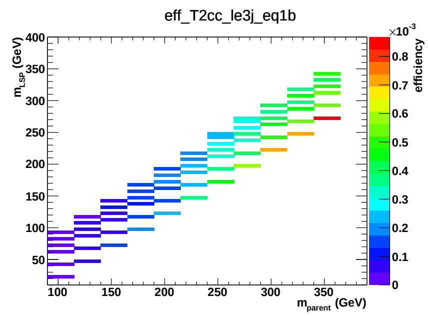

(b) Hadronic Selection Efficiency, (2–3,1)

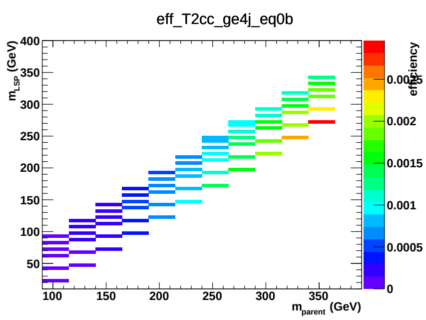

(c) Hadronic Selection Efficiency, (≥ 4,0)

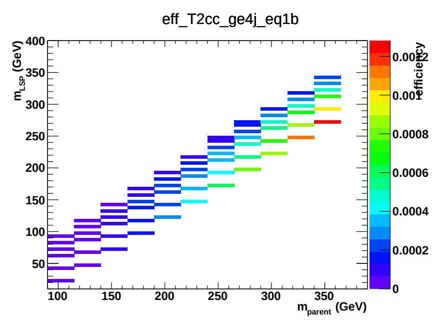

(d) Hadronic Selection Efficiency, (≥ 4,1)

Figure 12: Hadronic selection efficiency times acceptance for T2cc for the relevant event categories defined by n_{jet} and n_{b}. Note the different z-axis scales.

.3.2 T2tt

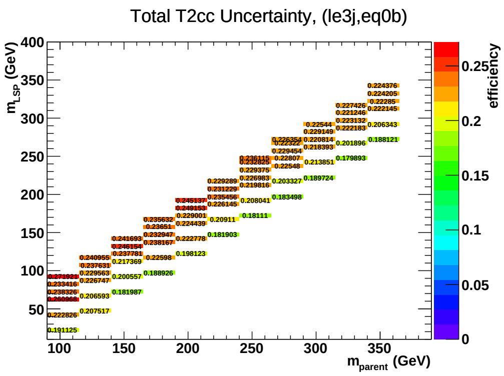

(a) $2 \leq n_{\mathrm{jet}} \leq 3$, $n_{\mathrm{b}} = 0$.

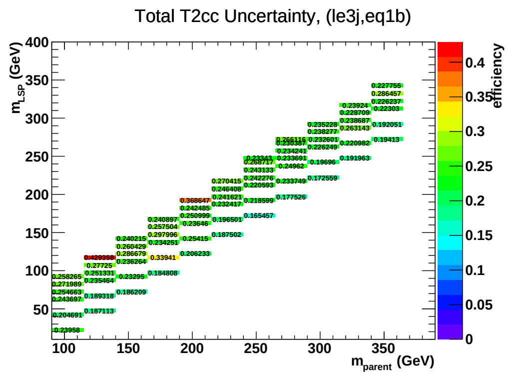

(b) $2 \leq n_{\mathrm{jet}} \leq 3$, $n_{\mathrm{b}} = 1$.

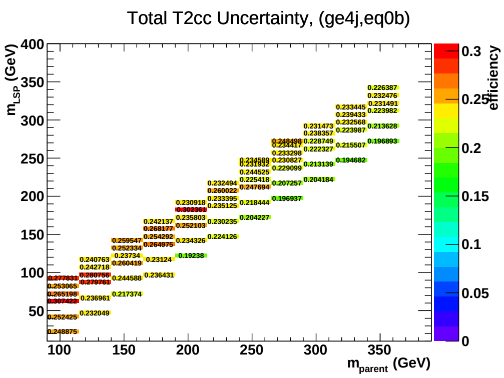

(c) $n_{\mathrm{jet}} \geq 4$, $n_{\mathrm{b}} = 0$.

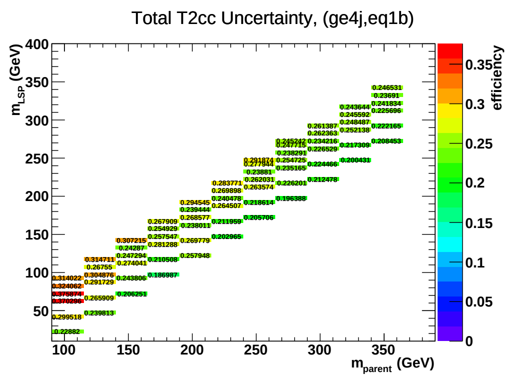

(d) $n_{\mathrm{jet}} \geq 4$, $n_{\mathrm{b}} = 1$.

Figure 13: The total systematic uncertainty in the signal efficiency times acceptance for all relevant event categories for the `T2cc` intepretation.

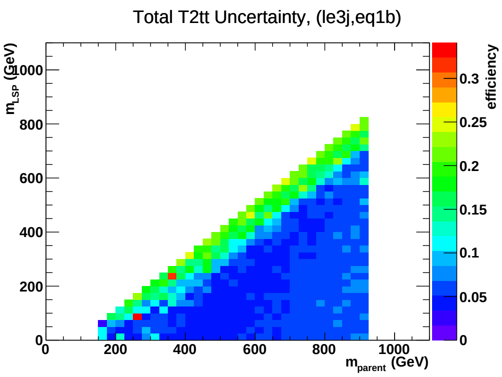

(a) $2 \leq n_{\text{jet}} \leq 3$, $n_{\text{b}} = 1$.

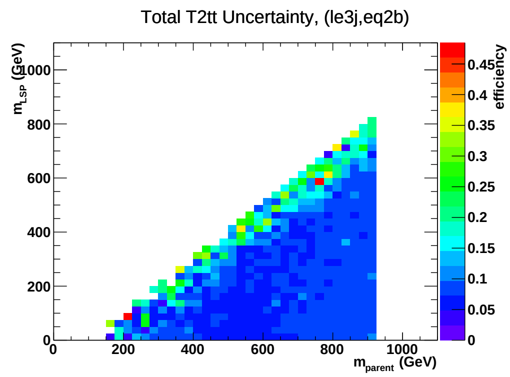

(b) $2 \leq n_{\text{jet}} \leq 3$, $n_{\text{b}} = 2$.

Figure 14: The total systematic uncertainty in the signal efficiency times acceptance for all relevant event categories for the `T2tt` intepretation.

.3.3 T2tt

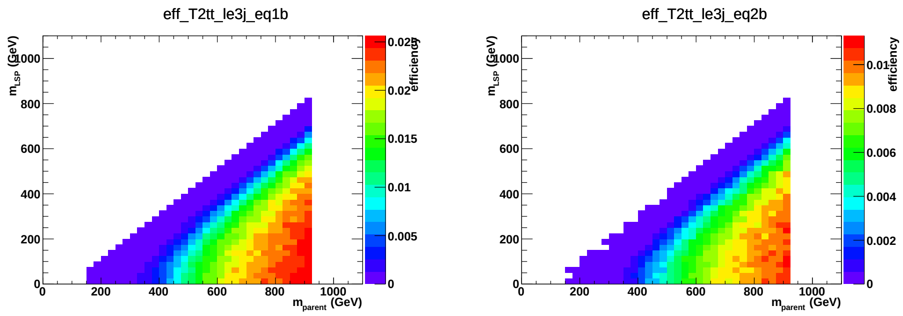

(a) Hadronic Selection Efficiency, (2–3,1) (b) Hadronic Selection Efficiency, (2–3,2)

Figure 15: Hadronic selection efficiency times acceptance for the `T2tt` for the relevant event categories defined by n_{jet} and n_{b}. Note the different z-axis scales.

Bibliography

[1] S. Chatrchyan et al. Missing transverse energy performance of the cms detector. *JINST*, 6:P09001, 2011.

[2] Serguei Chatrchyan et al. Determination of Jet Energy Calibration and Transverse Momentum Resolution in CMS. *JINST*, 6:P11002, 2011.

[3] V. Khachatryan et al. Search for Supersymmetry in pp Collisions at 7 TeV in Events with Jets and Missing Transverse Energy. *Phys. Lett. B*, 698:196, 2011.

[4] L. Randall and D. Tucker-Smith. Dijet searches for supersymmetry at the large hadron collider. *Phys. Rev. Lett.*, 101:221803, 2008.